INL/RPT-24-77405

Assessment of Readout Techniques for Passive Monitors

March 2024

Summary Report - M3CT-24IN0703011

Malwina Wilding and Kiyo Fujimoto
Idaho National Laboratory

Brian Jaques, David Estrada, and Josh Eixenberger
Boise State University

Idaho National Laboratory

INL is a U.S. Department of Energy National Laboratory operated by Battelle Energy Alliance, LLC

INL/RPT-24-77405

Assessment of Readout Techniques for Passive Monitors

Summary Report - M3CT-24IN07030

Malwina Wilding and Kiyo Fujimoto
Idaho National Laboratory
Brian Jaques, David Estrada, and Josh Eixenberger
Boise State University

March 2024

Idaho National Laboratory
Idaho Falls, Idaho 83415

http://www.inl.gov

Prepared for the
U.S. Department of Energy
Office of Nuclear Energy
Under DOE Idaho Operations Office
Contract DE-AC07-05ID14517

Page intentionally left blank

SUMMARY

This fiscal year (FY) 2023 report on passive temperature sensors covers two main objectives: to demonstrate that the optical dilatometer can successfully process disc-shaped silicon carbide (SiC) temperature monitors (TMs), and to demonstrate proof of concept for using the capacitance readout method to read printed melt wires. The SiC objective was successfully met by annealing and analyzing, via optical dilatometry, all eight 3-mm SiC discs provided by the Nuclear Science User Facilities (NSUF) Idaho State University (ISU) Nanostructured Steels for Enhanced Radiation Tolerance (N-SERT) experiment, which was irradiated at Idaho National Laboratory (INL)'s Advanced Test Reactor (ATR). Per the ISU N-SERT experiment, capsule 1 (KGT 3828-1 and KGT 3828-2) had a design temperature of 300°C +/- 50°C and an exposure of 2 dpa +/- 10%; capsule 2 (KGT 4600 and KGT 4609) had a design temperature of 300°C +/- 50°C and an exposure of 6 dpa +/- 10%; capsule 3 (KGT 4639-C and KGT 4639-D) had a design temperature of 500°C +/- 50°C and an exposure of 6 dpa +/- 10%; and capsule 4 (KGT 3841-3 and KGT 3841-4) had a design temperature of 500°C +/- 50°C and an exposure of 2 dpa +/- 10%. The target exposure rates, in dpa, are the neutron damage for various types of nanostructured steels. All but three SiC TMs (KGT 4600, KGT 4639-D, and KGT 3841-4) revealed averaged peak irradiation temperatures that fell within the design temperature ranges. The three SiC TMs that did not fall within the design temperatures ranges were at least 100°C below that target temperature. Furthermore, SiC TM KGT 3841-C revealed two irradiation regimes: one closer to the 300°C design temperature, and the other closer to the 500°C design temperature. Also, all the SiC TMs' averaged peak irradiation temperatures came in anywhere between 20°C and 240°C below the irradiation temperatures predicted by the thermal models. This showed the optical dilatometry method to be a reliable and less time-intensive process for determining averaged peak irradiation temperatures from passive SiC TMs such as rods and discs. Under the Advanced Sensors and Instrumentation (ASI) program in FY-23, Boise State University (BSU) proposed to demonstrate proof of concept for using a capacitance readout technique applicable to printed melt wires; however, they were stymied by the complexity of the capacitance readout method. In support of the BSU work, INL developed an additively manufactured (AM) ceramic package for encapsulating the new melt wires. Inks were synthesized at BSU that used new protocols rather than following previously established protocols implemented at INL, and testing of various temperatures was conducted at BSU to evaluate the melting behaviors of the printed melt wires. The result was that

the capacitance readout technique showed promise but also created more challenges than originally anticipated. For example, the tin ink synthesized at BSU showed unusual melting behaviors that did nothing to enhance the performance of the final printed melt wire prototype in terms of the capacitance readout method. To make the proof of concept work when applied to the printed melt wires, the ASI program would need to invest further resources and time. Consequently, the program is not planning to continue this proof of concept work in FY-24, based on the progress and findings achieved in FY-23.

ACKNOWLEDGEMENTS

This work was supported through the Nuclear Energy Enabling Technology (NEET) Advanced Sensor and Instrumentation (ASI) program and the Nuclear Science User Facilities (NSUF), under Department of Energy (DOE) Idaho Operations Office contract no. DE-AC07-05ID14517.

Page intentionally left blank

CONTENTS

FIGURES

TABLES

Page intentionally left blank

ACRONYMS

AM	Additive Manufactured
ASI	Advanced Sensors and Instrumentation
ATR	Advanced Test Reactor
BSU	Boise State University
DOE	Department of Energy
HFEF	The Hot Fuel Examination Facility
INL	Idaho National Laboratory
ISU	Idaho State University
MSL	Measurement Science Laboratory
MTR	Material Test Reactor
N-SERT	Nanostructured Steels for Enhanced Radiation Tolerance
NSUF	Nuclear Science User Facilities
PIE	Post-irradiation Examination
SiC	Silicon Carbide
TEM	Transmission Electron Microscopy
TM	Temperature Monitor

Page intentionally left blank

Assessment of Readout Techniques for Passive Monitors

1. INTRODUCTION

In April 2007, the U.S. Department of Energy (DOE) designated Idaho National Laboratory (INL)'s Advanced Test Reactor (ATR) as one of the National Scientific User Facilities (NSUF) for advancing U.S. leadership in nuclear science and technology. By attracting new users from various universities, laboratories, and industries, NSUF supports basic and applied nuclear research aimed at addressing national energy security needs. In support of this program, INL established in-house capabilities to develop, fabricate, test, and qualify new and enhanced temperature sensors for use in irradiation testing. This effort remains ongoing through DOE's Advanced Sensors and Instrumentation (ASI) program. Although most efforts emphasize sensors capable of providing real-time data, a select set of tasks has been completed to enhance passive sensors for irradiations in which instrumentation leads cannot be included (i.e., less expensive drop-in capsule tests).

The study of irradiation effects on material properties is a significant area of research regarding both fission and fusion systems. While neutron flux and energy spectrums are generally well understood, determining irradiation temperatures can be more challenging. Active (real-time) and passive (post-test evaluation) methods are employed for measuring temperatures in material test reactors (MTRs) such as INL's ATR, which offers exceptional materials testing capabilities for military, federal, university, and industry customers. Of the various temperature sensors being developed at INL, this report focuses on the passive temperature sensors currently being planned or deployed within the ASI program: namely, silicon carbide (SiC) temperature monitors (TMs) and printed melt wires. Thermocouples are generally used to provide real-time temperature indications in instrumented tests conducted at MTRs. Passive sensors such as SiC TMs and melt wires may be included in such tests as an independent method of detecting peak temperatures during irradiations. In less expensive static (drop-in) capsule tests, which have no leads attached for enabling real-time data transmission, melt wires and SiC TMs are essentially the only options for indicating peak irradiation temperatures.

Ever since the early 1960s, SiC has been used as a post-irradiation TM. Pravdyuk [1] first reported that neutron-induced lattice expansion of SiC annealed out whenever post-irradiation annealing temperature exceeds irradiation temperature. Snead [2] reported that this swelling had been associated with lattice dilation stemming from point defect formation. Among the many measurable properties of SiC TMs are electrical resistivity, thermal expansion, bulk density, thermal diffusivity, and lattice spacing. In general, thermal expansion measurement is an accepted post-irradiation measuring technique that has demonstrated ±20°C accuracy at up to 1600°C when determining peak irradiation temperatures. INL currently uses the continuous thermal expansion measurement technique to detect peak irradiation temperatures of up to 1200°C for SiC TMs. ([3]]-[5]) This INL approach was applied to the post-irradiation examination (PIE) of eight SiC TMs recently irradiated in the ATR and then evaluated at INL's Measurement Science Laboratory (MSL) as part of an NSUF experiment. The present paper discusses the use of SiC disc monitors at the ATR as well as the process employed to evaluate them at the MSL, and presents the measurements taken on the eight SiC 3-mm discs from the NSUF Idaho State University (ISU) Nanostructured Steels for Enhanced Radiation Tolerance (N-SERT) experiment (see Section 3).

Another method of determining irradiation temperatures involves including wires (i.e., standard melt wires or printed melt wires) of a known composition and melting temperature in the irradiation test. PIE is conducted on the wires to determine whether melting occurred, in turn indicating whether the corresponding melting temperature was reached (or exceeded). Such wire sensors are very useful for detecting abnormal temperature spikes during irradiation experiments (i.e., detecting whether a certain temperature was reached or exceeded during the irradiation test). Using in-house capabilities to verify the melting temperatures and suitability of candidate materials, INL, through the ASI program, is continually

expanding its library of available melt wires and the corresponding methods for reading them. The melt wire materials must also feature low neutron absorption cross sections, and all materials chosen for either the melt wires or the encapsulation thereof could potentially react with each other or with a vapor alloy generated by low eutectic points at high temperatures. To select an appropriate melt wire, it is important to evaluate the irradiation location type, applicable guidance from industry standards, and desirable attributes that would reduce the uncertainty associated with PIE. ([6]-[8]) Key insights from these evaluations are summarized in Section 4 of this paper. Finally, the conclusions reached regarding both types of passive sensors are covered in this report given in Section 5.

2. BACKGROUND

2.1 Silicon Carbide

Ever since the early 1960s, SiC has been used as a post-irradiation TM. Several researchers have observed that neutron-irradiation-induced lattice expansion of SiC anneals out when post-irradiation annealing temperatures exceed peak irradiation temperatures. Irradiation temperature is determined by measuring a property change after isochronal annealing or during a continuously monitored annealing process; and is considered the averaged peak irradiation temperature throughout an irradiation experiment. ([1]-[2]) INL has made significant efforts to implement continuous optical dilatometry as a new automated evaluation method. The optical dilatometer is automated, can anneal SiC TMs of various geometries and sizes (i.e., rods and discs), requires only a small amount of time to run, and saves valuable labor time in comparison to the traditional resistivity measurement method. [3]

Several limitations are imposed using SiC TMs. Temperatures are inferred via post-irradiation detection of material property changes (i.e., electrical resistivity and thermal expansion) that affect the stable defect population within SiC monitors that underwent irradiation. First, when irradiation temperatures rise during the latter part of an irradiation, it makes the SiC swelling saturate at low fluence—as well as for neutron damage levels exceeding 0.1 dpa—and the increasing temperature will anneal out defects that occur at the lower irradiation temperatures, while creating stable defects at the higher ones. When isochronal annealing is performed, any lower-temperature defects will, to some extent, already have been removed, and the recovery curve will be smeared to somewhat higher temperatures. This is why the measured irradiation temperatures for SiC TMs are averaged peak irradiation temperatures rather than the full range of temperatures detected throughout an irradiation. Second, when irradiation temperatures decrease during irradiation, it leads to defects being created and frozen-in at the higher temperature, while continuing to create lower-temperature defects as well. The isochronal anneal will then indicate the lowest irradiation temperature (in this case, found at the end of the irradiation period), and the recovery curve will be smeared because the annealing process will produce defects that persist at higher temperatures. However, as noted above, if irradiation tests are conducted at near or the same temperature (steady-state temperatures) when the reactor is at power (steady-state power), none of these situations should be of concern. ([3] &[4])

Figure 1 shows the SiC TMs that INL typically employs in both methods (i.e., electrical resistivity and continuous thermal expansion). Currently, INL uses either a SiC cylinder that is 1 mm in diameter (±0.05 mm) and 12.5 mm (±0.13 mm) in length, or SiC discs with an outer diameter of 3 or 5 mm (±0.05 mm) and a thickness of 1 mm (±0.13 mm). In past fiscal years (FYs), only SiC cylinders were measured in PIE; however, this report focuses on 3-mm SiC discs measured via optical dilatometry during PIE. [3]

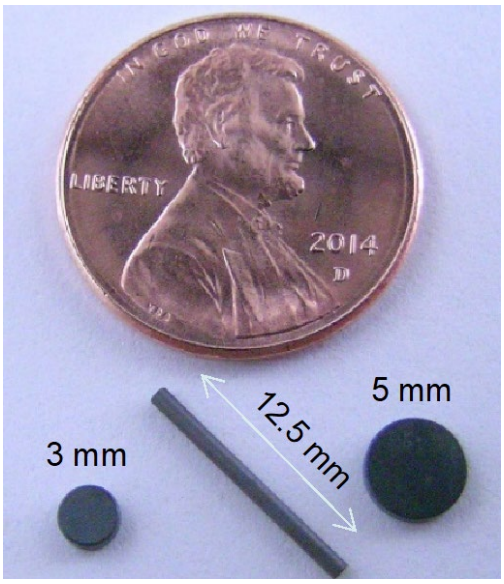

Figure 1. Two types of SiC TMs were available for use in the irradiation testing: small cylinders and discs. Only the discs were used for the purposes of this report. [3]

2.2 Melt Wires

Based on a meticulous material selection process combined with rigorous validation procedures, INL's MSL has produced a set of classical melt wire fabrication methods, including one that allows for encapsulating multiple wire materials into a single small-diameter quartz unit (see Figure 2). Over 40 qualified materials are stored at INL for use in melt wire fabrication, covering a temperature detection range of 29.73°C–1535°C. [15] While standard melt wires are commonly used in test reactor experiments supported by MTRs (e.g., the ATR), the sensor design is constrained by the predesigned capsules, whose geometries are in turn imposed by the layout of the MTR core. These capsules may only allow for sensors that are a couple of millimeters in diameter and feature prespecified geometries, and placing multiple specimens simultaneously within the capsules may leave little to no space for instrumentation.

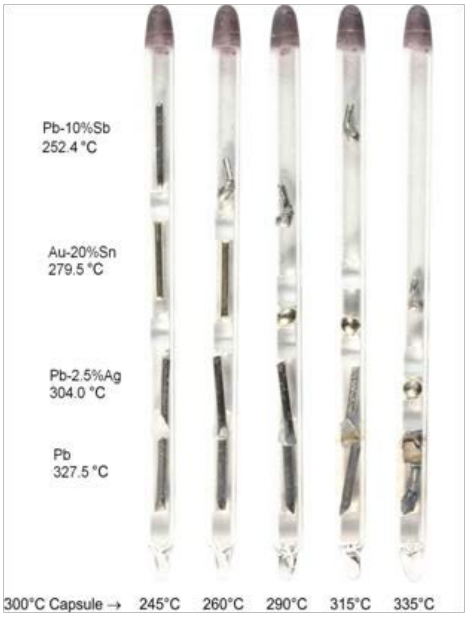

Figure 2. Typical quartz-encapsulated melt wire progression. [15]

Production of robust miniature sensors is enabled via additive manufacturing techniques such as aerosol jet printing, inkjet printing, and micro-dispense printing. Incorporating these technologies fosters the development of ASI for reactors and fuel-cycle facilities, with printing patterns as small as 10 µm. These feature sizes aid in device miniaturization, especially considering that traditional melt wire capsules typically require a wire length of approximately 2 mm. Through the advanced manufacturing portion of the ASI program, novel technologies such as aerosol jet printing are being explored for use in the development of unique sensors otherwise unobtainable via conventional fabrication processes. Past advanced manufactured melt wire development efforts and corresponding challenges are covered in ([16]-[18]). The development efforts conducted during FY-22 focused on further improving the melt wire encapsulation design and the material compatibility between the melt wire arrays and the encapsulation container. The goal was to improve the readability of the x-ray computed tomography (XCT) results and to minimize neutron activation of the printed melt wire package. Ultimately, the material selected for the encapsulation container was vanadium. A printed ceramic sublayer (alumina disc) was introduced into the encapsulation, and the aerosol-jet-printed melt wires were created out of indium with a melting point of 157°C, indium/silver (96/4 at%) with a melting point of 219°C, and tin with a melting point of 230°C (see Figure 3). [18]

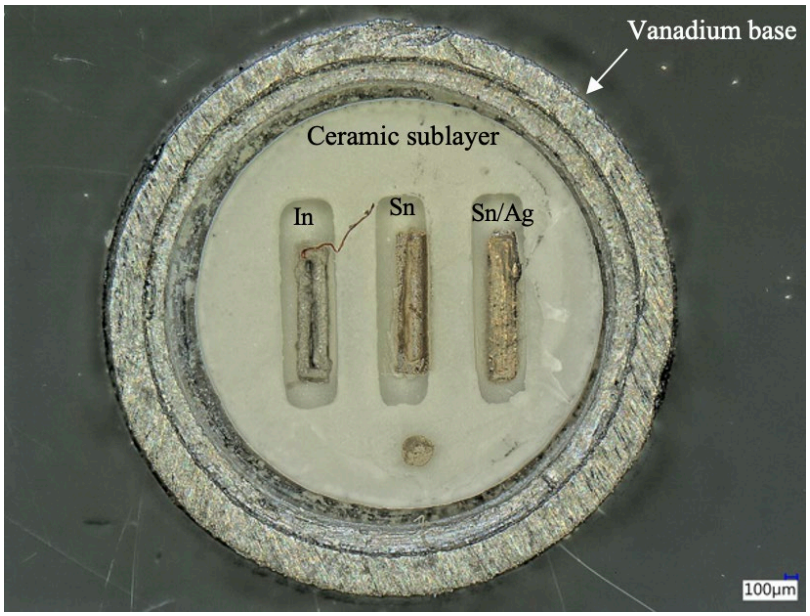

Figure 3. Printed melt wires on a ceramic sublayer placed inside the vanadium base (from FY-22). [18]

A limiting factor in previous work regarding printed melt wires was the readout technology, with the current metal packaging limiting the readout of melt wires to use of XCT. The XCT is inaccessible and cost prohibitive, and visual inspection is not an option with metal packaging. Thus, under the ASI program in FY-23, Boise State University (BSU) proposed to demonstrate proof of concept for a capacitance readout technique applicable to printed melt wires. In support of that work, INL developed an AM ceramic package for encapsulating the new melt wires. Inks were synthesized at BSU that used new protocols rather than following previously established protocols implemented at INL, and testing at various temperatures was conducted to evaluate the melt behavior of the printed melt wires. An electrical readout pattern, shown in Figure 4, was developed so that the sensors could be read from within the package as part of preliminary investigation into melt capacitors. For FY-23, BSU used an interdigitated structure for the capacitive device, and an LCR meter to read the capacitance before and after furnace testing that would determine whether the printed melt wire melted or not. All the details on BSU's FY-23 contributions to the ASI program are given in Appendix A of this report.

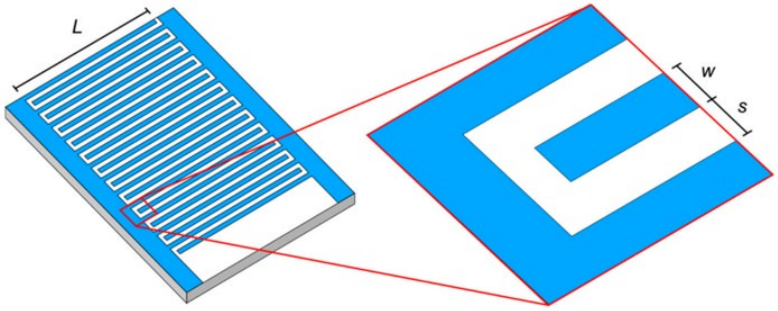

Figure 4. Interdigitated electrode pattern created using finite-element models of the FY-23 printed melt wires.

3. SILICON CARBIDE TEMPERATURE MONITORS

3.1 Nuclear Science User Facilities Idaho State University Nanostructured Steels for Enhanced Radiation Tolerance Experiment

NSUF's mission is to provide nuclear energy researchers with access to world-class capabilities and to facilitate the advancement of nuclear science and technology. An NSUF irradiation and examination experiment at ATR, awarded under NSUF number ISU-10537 and named N-SERT, was conducted in collaboration with ISU, with Dr. Haiming Wen serving as the principal investigator. The purpose of this drop-in capsule experiment was to establish the irradiation performance of ultrafine-grained and nanocrystalline variations of reactor structural and cladding steels produced using severe plastic deformation manufacturing techniques. Applying microstructural engineering to improve the performance of currently used steels via advanced manufacturing techniques shows great potential for improving radiation tolerances—and doing so at relatively low cost in comparison to the development of new alloys. Austenitic steels are very important core internal materials for light-water reactors, and ferritic/martensitic steels are the leading fuel cladding and structural materials for advanced test reactors. One way to measure irradiation temperature is via passive TMs such as melt wires and SiC TMs. Figure 5 shows how each passive SiC TM was positioned inside the four ISU N-SERT capsules. [19] Table 1 shows the thermal model estimates of the transmission electron microscope (TEM) specimen temperatures, where the SiC discs were placed, for each capsule. [20]

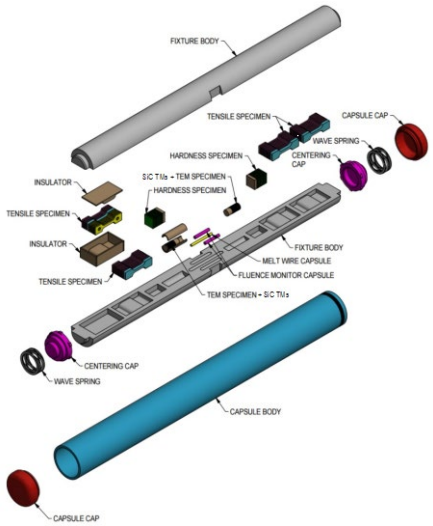

Figure 5. Typical ISU N-SERT capsule assembly, including the locations of the SiC and melt-wire TMs. [19]

Table 1. ISU N-SERT irradiation conditions and estimated temperatures for TEM specimens based on the thermal models. [20]

Capsule Number	Target Temp. [°C]	Capsule Temp. Estimates [°C]	HFEF Identification	Temperature Estimates for SiC [°C]		
				T min	T max	Avg
1	300+/-50	318-337	KGT 3828-1	336	337	336.5
			KGT 3828-2	333	335	334
2	300+/-50	323-347	KGT 4600	345	347	346

			KGT 4609	341	343	342
3	500+/-50	482-511	KGT 4639-C	506	507	506.5
			KGT 4639-D	499	501	500
4	500+/-50	489-526	KGT-3841-3	517	519	518
			KGT 3841-4	509	511	510

3.2 Silicon Carbide Discs

The quality of the material used to manufacture the SiC TMs greatly impacts the radiation-induced swelling and in turn the ensuing peak irradiation temperature evaluation. The SiC TMs are produced via a chemical vapor deposition process that allows a high level of purity (99.9995%) and a density close to the theoretical, meaning that no voids or micro cracks are detected. Due to its polycrystalline β-cubic structure, SiC's material characteristics are isotropic. Based on these characteristics, the SiC TMs are manufactured to exceed a resistivity of 1000 ohm/m. A total of eight SiC TMs had been irradiated as part of NSUF's ISU N-SERT experiment at ATR, [19] with target doses of 2 dpa (capsules 1 and 4) and 6 dpa (capsules 3 and 4) (within +/-10%), and target temperatures of 300°C (capsules 1 and 4) and 500°C (capsules 2 and 3) (within +/-50°C) for stainless steel specimens. The target exposure rates, in dpa, are the neutron damage for various types of nanostructured steels. These SiC TMs are listed in Table 2.

Table 2. SiC TM MSL/HFEF identification names, capsule numbers, target design temperatures, and exposure levels, along with the positioning of each capsule in the ATR.

SiC Number	MSL Identification	HFEF Identification	Capsule Number	Design Temperature [°C]	Exposure [dpa]	Capsule Position in ATR
1	HTTL-244L2-R1	KGT 3828-1	1	300 +/- 50	2 +/- 10%	Top
2	HTTL-243U1	KGT 3828-2				
3	HTTL-242L1-R1	KGT 4600	2	300 +/- 50	6 +/- 10%	Middle Top
4	HTTL-244-U2	KGT 4609				
5	HTTL-243L1-R1	KGT 4639-C	3	500 +/- 50	6 +/- 10%	Middle Bottom
6	HTTL-243L2	KGT 4639-D				
7	HTTL-241L2	KGT-3841-3	4	500 +/- 50	2 +/- 10%	Bottom
8	HTTL-242U2	KGT-3841-4				

3.3 Optical Dilatometry Method

A TA Instruments DIL 806 optical dilatometer was used for PIE of the SiC TMs to determine their averaged peak irradiation temperatures. The DIL 806 is a contactless dilatometric measurement system that allows the SiC TMs to freely expand/shrink without any interference from mechanical contact. This fosters a more precise determination of the passive monitor's dimensional changes and the temperature at which the changes are detected. Furthermore, avoidance of any load caused by contact with a measuring system enables the analysis to be extended well beyond the softening point into the melt. Additionally, the optical dilatometer offers effective environmental control during the testing, enabling users to analyze samples not only in air but also under a vacuum or in an inert atmosphere—a key requirement for avoiding any oxidization issues involving the SiC TMs. The related equipment and processes are comprehensively described in [3].

Each dilatometer run begins at room temperature and gradually increases at a rate of 1°C per minute until it reaches approximately 300°C above the anticipated irradiation temperature. (For all eight ISU N-SERT SiC TMs, the annealing dilatometer run was set to reach 800°C, as shown in Figure 6.) It is then maintained at this temperature for 5 minutes before being cooled back down to room temperature at the same rate of 1°C per minute. SiC TMs can undergo annealing in the optical dilatometer, where the peak irradiation temperature can be evaluated from 100°C to 1200°C with accuracies of ±20°C. [3] The results shown in Figure 6 correspond to a dilatometer run for KGT 4609, a SiC TM irradiated in the ATR as part of an NSUF ISU N-SERT experiment. Near-identical temperatures were recorded between the furnace and the sample; therefore, the furnace temperature was selected as the primary control parameter for the optical dilatometer run. Moreover, the power output displayed a largely consistent pattern throughout the entire run, and in this regard all eight SiC TMs aligned with expectations.

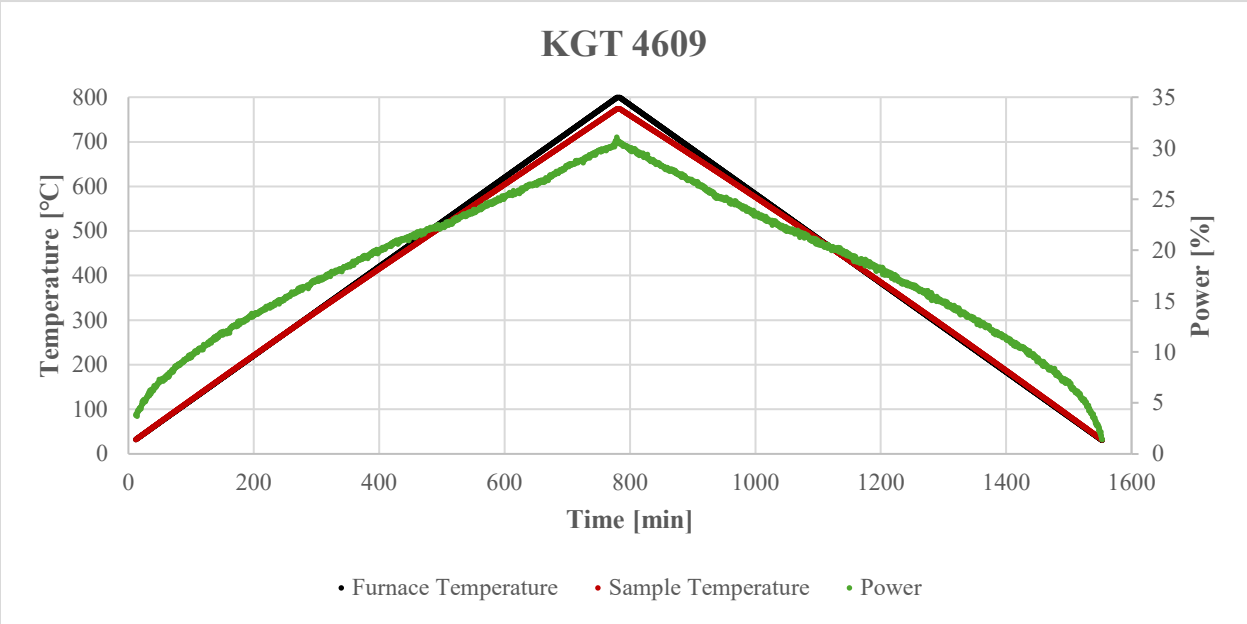

Figure 6. Temperature profiles of the furnace, sample controls, and power for SiC TM KGT 4609.

SiC TMs exposed to reactor irradiation experience an increase in volume due to radiation-induced swelling, as observed by Snead. [2] Furthermore, little change in the crystal volume is expected at annealing temperatures lower than the irradiation temperature, but a decrease in volume is expected when the annealing temperature surpasses the irradiation temperature. This is demonstrated in Table 3, with the TM length increasing post-irradiation by an average of ~28 µm, followed by a length decrease of ~11 µm following the annealing process in the dilatometer.

Table 3. SiC TM changes in length both pre- and post-irradiation, and after annealing in the dilatometer (post-PIE).

SiC Number	Length [µm]				
	Pre-Irradiation	Post-Irradiation	ΔLength	Post-Annealing	ΔLength
1	3000	3030.8	30.8	3020.3	-10.5
2	3000	3031.4	31.4	3018.3	-13.1
3	3000	3031.4	31.4	3017.3	-14.1
4	3000	3023.2	23.2	3009.9	-13.3

5	3000	3021.7	21.7	3016.1	-5.6
6	3000	3027.5	27.5	3017.6	-9.9
7	3000	3030.8	30.8	3013.4	-17.4
8	3000	3026.6	26.6	3020.8	-5.8
Average	3000.0	3027.9	27.9	3016.7	-11.2

3.4 Silicon Carbide Results

3.4.1 KGT 3828-1 (Capsule 1)

Figure 7 plots the difference between the heating and the cooling changes in length for ISU N-SERT SiC TM KGT 3828-1, based on data collected from an optical dilatometer run. The target (design) temperature for KGT 3828-1 was 300°C +/- 50°C, with a neutron exposure of 2 dpa for stainless steel specimens; additionally, the thermal model estimated the SiC temperatures to reach between 336°C and 337°C during the ATR irradiation. The first step of determining irradiation temperature required fitting a straight line (orange line) to the relatively straight section of the length change curve below the design temperature of 300°C, as shown in Figure 7. The second step involved fitting a straight line (shown in black) to the data above the design temperature (red dot). The third (green line) fitted line was centered around where the data began curving downward subsequently the flat region below the design temperature. The intersection of the orange and black lines was specified as the maximum irradiation temperature (yellow square) of 270°C, whereas the minimum irradiation temperature (i.e., 220°C) was specified as the intersection of the green and orange lines (green circle). This measurement method was also used for the seven remaining ISU N-SERT SiC discs. As a result, Figure 7 reveals the averaged peak irradiation temperature (T max) to be 270°C +/- 20°C, with the irradiation temperature at steady-state reactor power starting at about 220°C. As a result, SiC TM KGT 3828-1's averaged peak irradiation temperature was within the target temperature, and roughly 50°C to 90°C below the estimated SiC temperatures derived using thermal models.

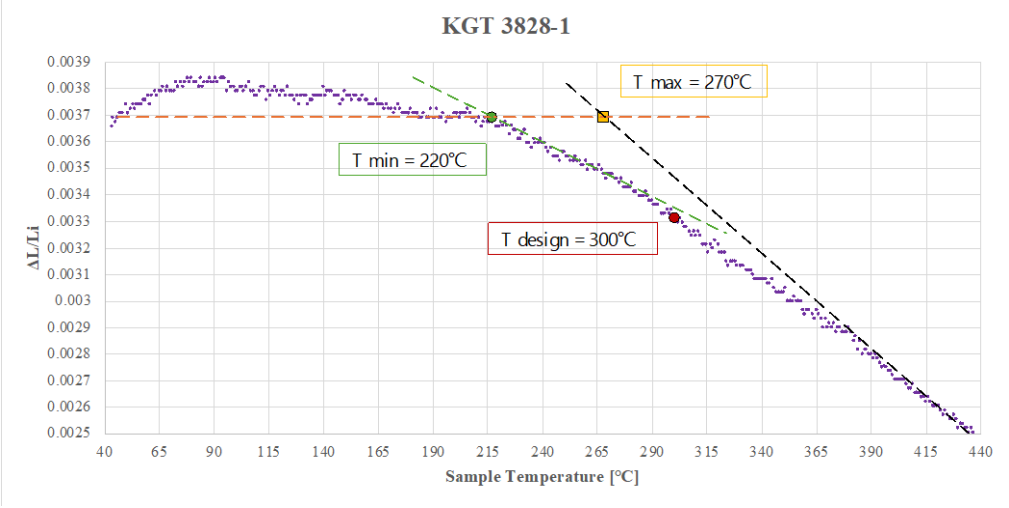

Figure 7. Irradiation temperatures based on the delta change in length and the target (design) temperature of SiC TM KGT 3828-1.

3.4.2 KGT 3828-2 (Capsule 1)

Figure 8 plots the difference between the heating and the cooling changes in length for ISU N-SERT SiC TM KGT 3828-2, based on data collected from an optical dilatometer run. The target (design)

temperature for KGT 3828-2 was 300°C +/- 50°C, with a neutron exposure of 2 dpa for stainless steel specimens; additionally, the thermal model estimated SiC temperatures to reach between 333°C and 335°C during the ATR irradiation. Figure 8 reveals the averaged peak irradiation temperature (T max) to be 230°C +/- 20°C, with the irradiation temperature at steady-state reactor power starting at about 180°C. As a result, SiC TM KGT 3828-2's averaged peak irradiation temperature came in below the target temperature by anywhere between 40° and 100°C, and roughly 85°C to 120°C below the estimated SiC temperature derived using thermal models.

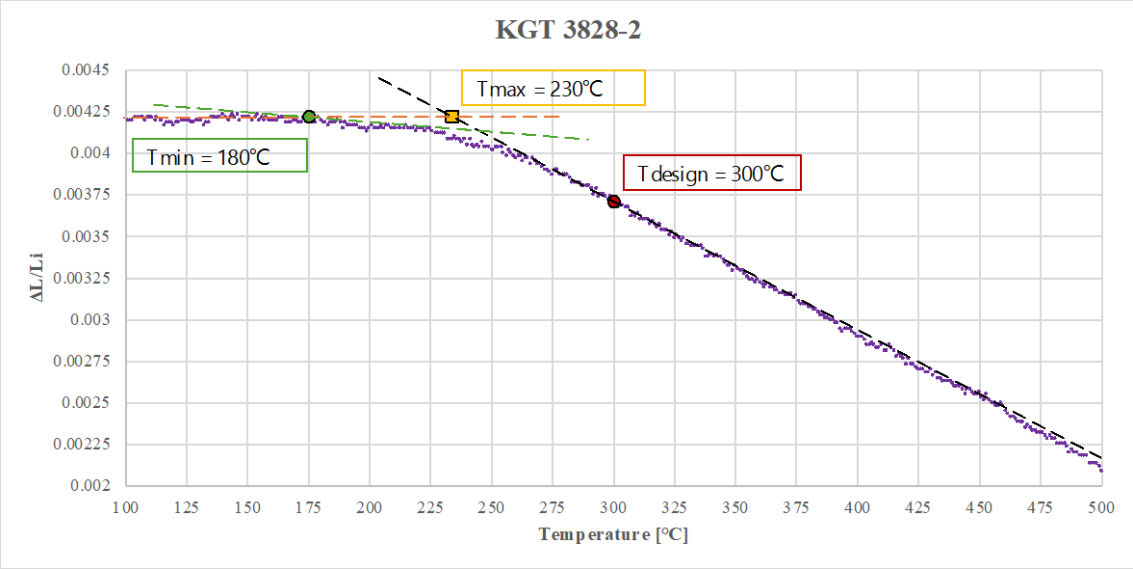

Figure 8. Irradiation temperatures based on the delta change in length and the target (design) temperature of SiC TM KGT 3828-2.

3.4.3 KGT 4600 (Capsule 2)

Figure 9 plots the difference between the heating and the cooling changes in length for ISU N-SERT SiC TM KGT 4600, based on data collected from an optical dilatometer run. The target (design) temperature for KGT 4600 was 300°C +/- 50°C, with a neutron exposure of 6 dpa for stainless steel specimens; additionally, the thermal model estimated SiC temperatures to reach between 345°C and 347°C during the ATR irradiation. Figure 9 reveals the averaged peak irradiation temperature (T max) to be 200°C +/- 20°C, with the irradiation temperature at steady-state reactor power starting at about 190°C. As a result, SiC TM KGT 4600's averaged peak irradiation temperature came in below the target temperature by anywhere between 70° and 130°C, and roughly 130°C to 165°C below the estimated SiC temperature derived using thermal models.

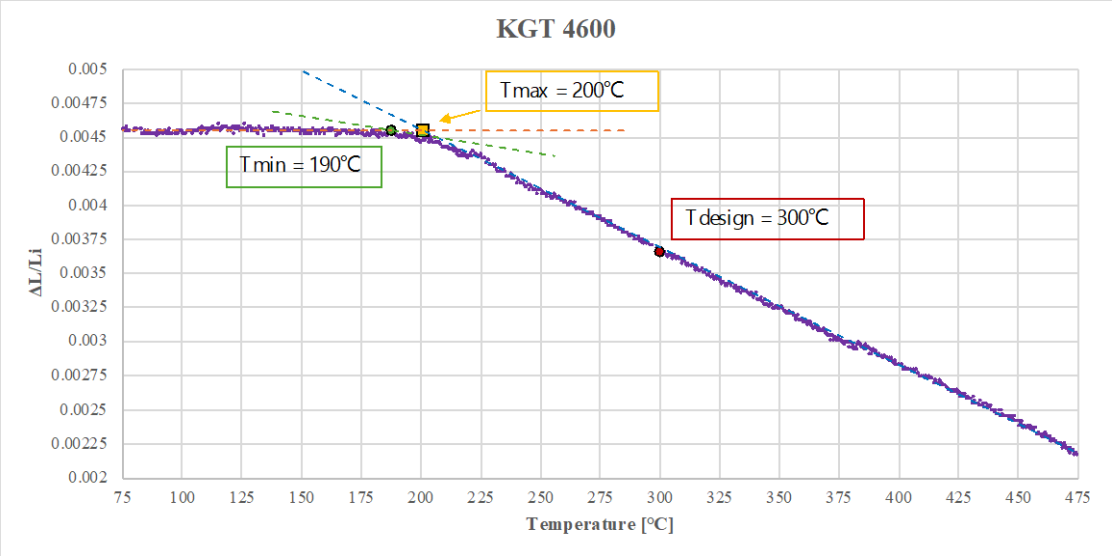

Figure 9. Irradiation temperatures based on the delta change in length and the target (design) temperature of SiC TM KGT 4600.

3.4.4 KGT 4609 (Capsule 2)

Figure 10 plots the difference between the heating and the cooling changes in length for ISU N-SERT SiC TM KGT 4609, based on data collected from an optical dilatometer run. The target (design) temperature for KGT 4609 was 300°C +/- 50°C, with a neutron exposure of 6 dpa for stainless steel specimens; additionally, the thermal model estimated SiC temperatures to reach between 341°C and 343°C during the ATR irradiation. Figure 10 reveals the averaged peak irradiation temperature (T max) to be 300°C +/- 20°C, with the irradiation temperature at steady-state reactor power starting at about 260°C. As a result, SiC TM KGT 4609's averaged peak irradiation temperature was within the target temperature, and roughly 20°C to 60°C below the estimated SiC temperatures derived using thermal models.

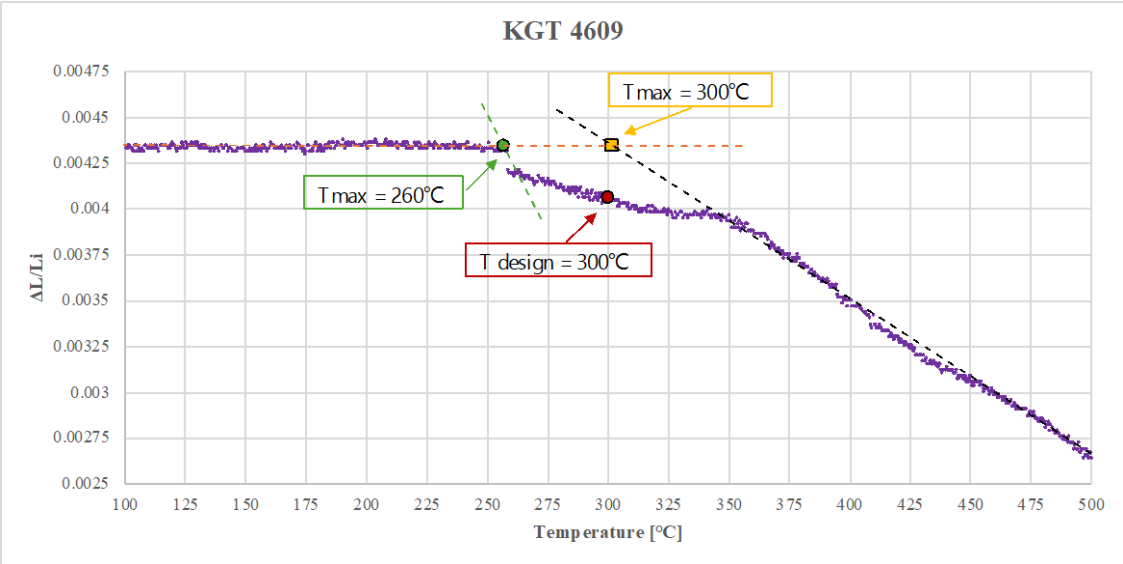

Figure 10. Irradiation temperatures based on the delta change in length and the target (design) temperature of SiC TM KGT 4609.

3.4.5 KGT 4639-C (Capsule 3)

Figure 11 plots the difference between the heating and the cooling changes in length for ISU N-SERT SiC TM KGT 4639-C, based on data collected from an optical dilatometer run. The target (design) temperature for KGT 4639-C was 300°C +/- 50°C, with a neutron exposure of 6 dpa for stainless steel specimens; additionally, the thermal model estimated SiC temperatures to reach between 506°C and 507°C during the ATR irradiation. Figure 11 reveals the averaged peak irradiation temperature (T max) to be 440°C +/- 20°C, with the irradiation temperature at steady-state reactor power starting at about 410°C. As a result, SiC TM KGT 4639-C's averaged peak irradiation temperature was within the target temperature, and roughly 50°C to 90°C below the estimated SiC temperatures derived using thermal models.

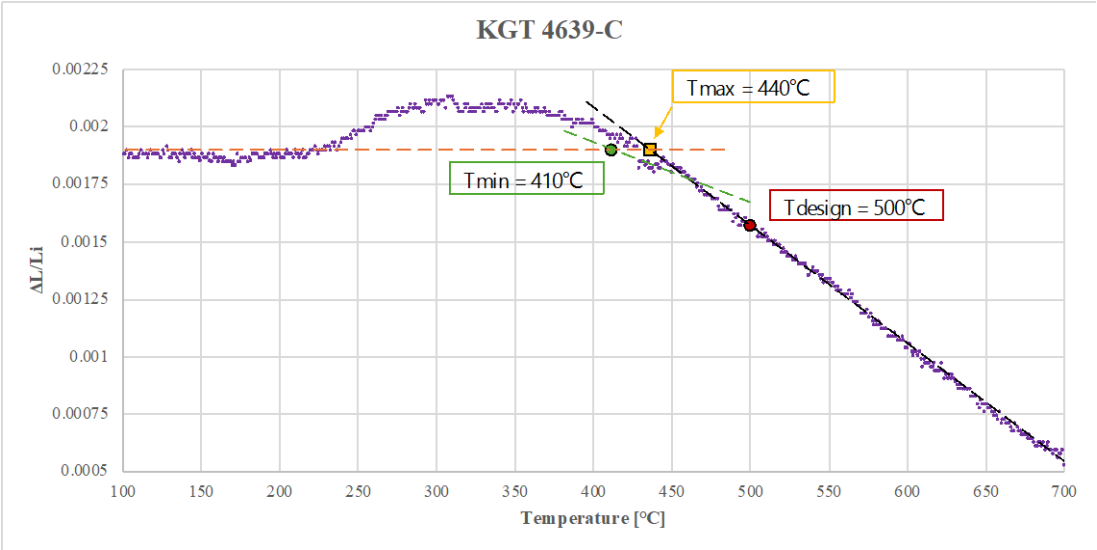

Figure 11. Irradiation temperatures based on the delta change in length and the target (design) temperature of SiC TM KGT 4639-C.

3.4.6 KGT 4639-D (Capsule 3)

Figure 12 plots the difference between the heating and the cooling changes in length for ISU N-SERT SiC TM KGT 4639-D, based on data collected from an optical dilatometer run. The target (design) temperature for KGT 4639-D was 500°C +/- 50°C, with a neutron exposure of 6 dpa for stainless steel specimens; additionally, the thermal model estimated SiC temperatures to reach between 499°C and 501°C during the ATR irradiation. Figure 12 reveals the averaged peak irradiation temperature (T max) to be 280°C +/- 20°C, with the irradiation temperature at steady-state reactor power starting at about 260°C. As a result, SiC TM KGT 4639-D's averaged peak irradiation temperature came in below the target temperature by anywhere between 190° and 250°C, and roughly 200°C to 240°C below the estimated SiC temperatures derived using thermal models.

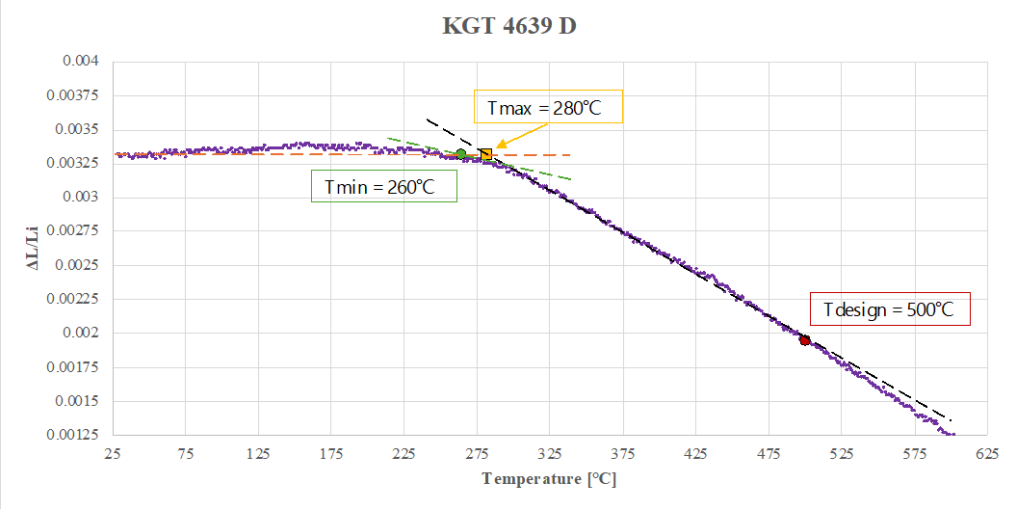

Figure 12. Irradiation temperatures based on the delta change in length and the target (design) temperature of SiC TM KGT 4639-D.

3.4.7 KGT 3841-3 (Capsule 4)

Figure 13 plots the difference between the heating and the cooling changes in length for ISU N-SERT SiC TM KGT 4841-3, based on data collected from an optical dilatometer run. The target (design) temperature for KGT 4841-3 was 500°C +/- 50°C, with a neutron exposure of 2 dpa for stainless steel specimens; additionally, the thermal model estimated SiC temperatures to reach between 517°C and 519°C during the ATR irradiation. Figure 13 reveals the presence of two irradiation temperature regimes. The first (lower irradiation) regime has an averaged peak irradiation temperature (T max 1) of 310°C +/- 20°C, with the irradiation temperature at steady-state reactor power starting at about 300°C. The second (higher irradiation) regime has an averaged peak irradiation temperature (T max 2) of 480°C +/- 20°C, with the irradiation temperature at steady-state reactor power starting at about 420°C. Thus, SiC TM KGT 3841-3 experienced two irradiation temperature regimes during the ATR irradiation. The first (lower averaged) peak irradiation temperature came in below the target temperature by anywhere between 160°C and 220°C, and roughly 190°C to 230°C below the estimated SiC temperatures derived using thermal models. The second (higher averaged) peak irradiation temperature was within the target temperature, and roughly 20°C to 60°C below the estimated SiC temperatures derived using thermal models.

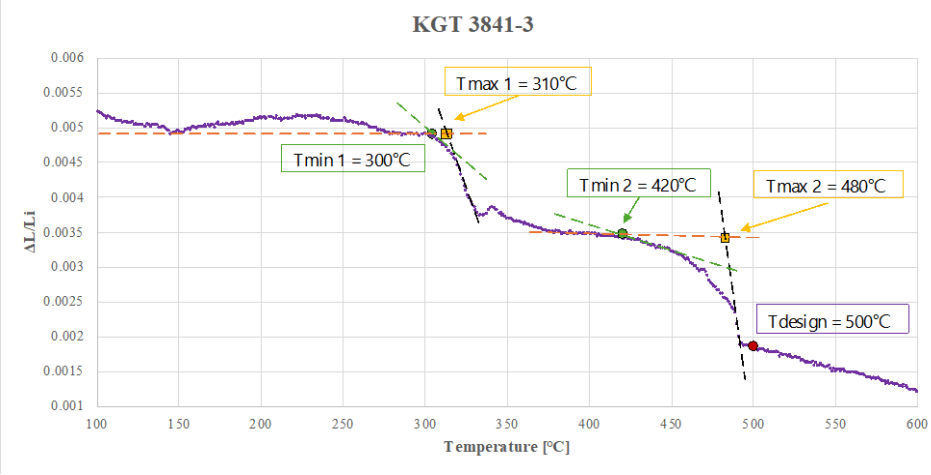

Figure 13. Irradiation temperatures based on the delta change in length and the design temperature of SiC TM KGT 3841-3.

3.4.8 KGT 3841-4 (Capsule 4)

Figure 14 plots the difference between the heating and the cooling changes in length for ISU N-SERT SiC TM KGT 3841-4-D, based on data collected from an optical dilatometer run. The target (design) temperature for KGT 3841-4 was 500°C +/- 50°C, with a neutron exposure of 2 dpa for stainless steel specimens; additionally, the thermal model estimated SiC temperatures to reach between 509°C and 511°C during the ATR irradiation. Figure 14 reveals the averaged peak irradiation temperature (T max) to be 410°C +/- 20°C, with the irradiation temperature at steady-state reactor power starting at about 360°C. As a result, SiC TM KGT 3841-4's averaged peak irradiation temperature came in below the target temperature by anywhere between 60°C and 120°C, and roughly 80°C to 120°C below the estimated SiC temperatures derived using thermal models.

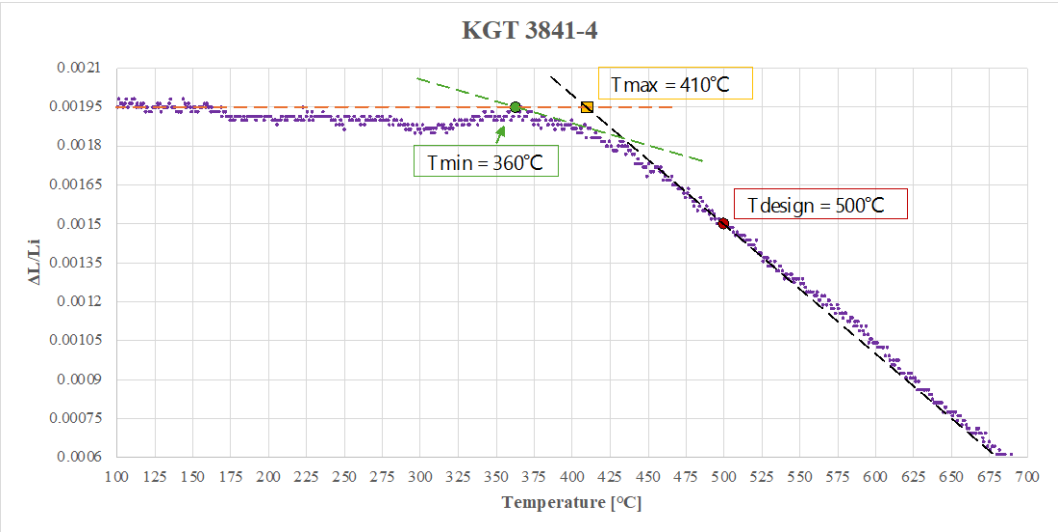

Figure 14. Irradiation temperatures based on the delta change in length and the target (design) temperature of SiC TM KGT 3841-4.

4. PRINTED MELT WIRES

Under the ASI program in FY-23, BSU proposed to demonstrate proof of concept for a capacitance readout technique applicable to printed melt wires. In support of this BSU work, INL developed an AM ceramic package for encapsulating the new melt wires. This package is described in Section 4.1. Inks were synthesized at BSU that used new protocols rather than following previously established protocols implemented at INL, and testing at various temperatures was conducted to evaluate the melt behavior of the printed melt wires. All the details on BSU's FY-23 contributions to the ASI program are given in Appendix A of this report. The capacitance readout technique showed promise but also created more challenges than originally anticipated. For example, the tin inks synthesized at BSU showed unusual melting behaviors that did nothing to enhance the performance of the final printed melt wire prototype in terms of the capacitance readout method. To make the proof of concept work when applied to the printed melt wires, the ASI program would need to invest further resources and time. Consequently, the program is not planning to continue this proof of concept work in FY-24, based on the progress and findings achieved in FY-23 (Appendix A).

4.1 Ceramic Encapsulation

The ceramic encapsulation was designed in SOLIDWORKS, and the printed foils were created using digital light projection on an Admatech A130 with an alumina slurry (Admaprint A130). The green body was then subjected to debinding and sintering to remove the organic binders and initial porosity to establish the defining microstructure and material properties. This process began by submerging the prints in water for 24 hours at 30°C to remove as much of the water-soluble components in the resin as possible. After soaking, the forms were wiped with a soft brush to remove any non-cured resin on the print surface. Next, the forms were dried in air for 24 hours. During the debinding step, organic components (binders) were removed via exposure to high temperatures; for the alumina, the following debinding heating profile was used: (1) starting at room temperature, ramp the furnace to 150°C at a rate of 60°C/hour; (2) remain at 150°C for 30 minutes; (3) ramp the furnace to 450°C at a rate of 12°C/hour; (4) ramp the furnace to 1000°C at a rate of 60°C/hour; (5) remain at 1000°C for 120 minutes; and (6) bring the furnace back down to room temperature at a rate of 100°C/hour. Once the debinding step was completed, the pieces were sintered to allow the alumina particles within the print to come in close contact with each other. This increases the density of the print and thus shrinks its overall dimensions. The sintering step was completed using the following heating profile: (1) starting at room temperature, ramp the furnace to 1000°C at a rate of 200°C/hour; (2) remain at 100°C for 30 minutes; (3) ramp the furnace to 1575°C at a rate of 100°C/hour; (4) perform a second ramp to 1625°C at 75°C/hour; (5) remain at 1625°C for 120 minutes; and (6) bring the furnace down to room temperature at a rate of 300°C/hour. The final product is seen in Figure 15.

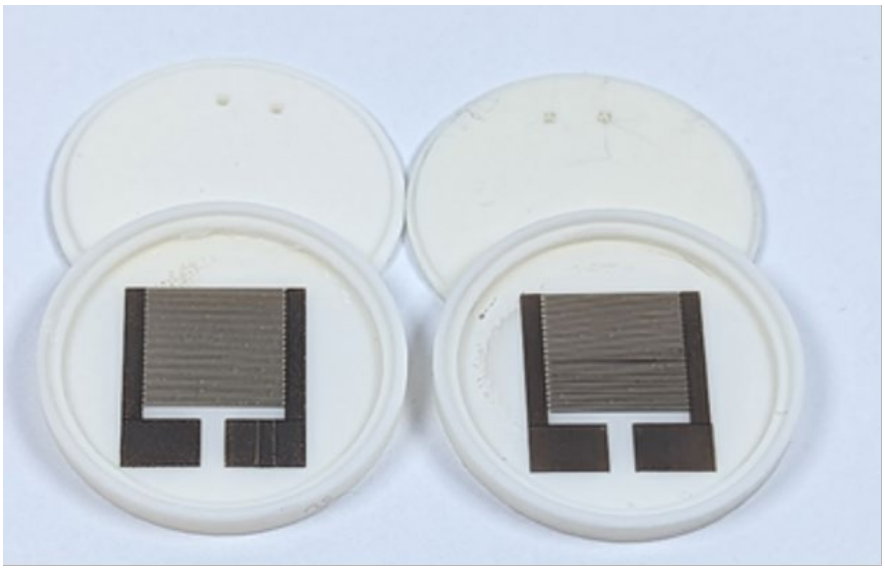

Figure 15. Ceramic encapsulation discs for the printed melt wire package.

5. CONCLUSION

In conclusion, the development and implementation of passive temperature sensors play a crucial role in advancing nuclear science and technology. INL's ATR, which carries a NSUF designation, supports basic and applied nuclear research to address national energy security needs. Under DOE's ASI program, INL established in-house capabilities for the development and qualification of temperature sensors usable for irradiation testing. One type of passive temperature sensor discussed in this report is the SiC TM. This sensor uses post-irradiation annealing and the measurement of properties such as thermal expansion to determine peak irradiation temperatures. These sensors have been extensively researched and deployed for several decades now, offering accurate temperature measurement capabilities within specific temperature ranges (accuracies of ±20°C). However, the limiting factor is that it can only detect the averaged peak irradiation temperature and not any low/high temperature spikes that occur over the course of an irradiation.

The first objective of this report was to demonstrate that the optical dilatometer can successfully process disc-shaped SiC TMs. The SiC objective was successfully met by annealing and analyzing, via optical dilatometry, all eight 3-mm SiC discs provided by the NSUF ISU N-SERT experiment, which was irradiated at ATR. The optical dilatometer is automated, requires only a small amount of time to run, and is easy to use, thus saving valuable labor time in comparison to the traditional resistivity measurement method. Per the ISU N-SERT experiment, capsule 1 (KGT 3828-1 and KGT 3828-2) had a design temperature of 300°C +/- 50°C and an exposure of 2 dpa +/- 10%; capsule 2 (KGT 4600 and KGT 4609) had a design temperature of 300°C +/- 50°C and an exposure of 6 dpa +/- 10%; capsule 3 (KGT 4639-C and KGT 4639-D) had a design temperature of 500°C +/- 50°C and an exposure of 6 dpa +/- 10%; and capsule 4 (KGT 3841-3 and KGT 3841-4) had a design temperature of 500°C +/- 50°C and an exposure of 2 dpa +/- 10%. The target exposure rates, in dpa, are the neutron damage for various types of nanostructured steels. All but three SiC TMs (KGT 4600, KGT 4639-D, and KGT 3841-4) revealed averaged peak irradiation temperatures that fell within the design temperature ranges (see Table 4). The three SiC TMs that did not fall within the design temperature ranges were at least 100°C below that target temperature. Furthermore, SiC TM KGT 3841-C revealed two irradiation regimes: one closer to the 300°C design temperature, and the other closer to the 500°C design temperature. Furthermore, all the SiC TMs' averaged peak irradiation temperatures were anywhere between 20°C and 240°C below the irradiation temperatures predicted by the thermal models.

Table 4. SiC TM HFEF identification names, design temperatures, thermal model temperature predictions, peak irradiation temperatures, and whether the SiC irradiation temperatures met the design and thermal model temperature predictions.

HFEF Identification	Design Temp. [°C]	Thermal Model Avg. Temp. [°C]	Avg. Peak Irradiation Temp. [°C]	Met Design Temp.	Met Thermal Model Avg. Temp.
KGT 3828-1	300+/-50	336.5	270+/-20	YES	Below
KGT 3828-2	300+/-50	334	230+/-20	YES	Below
KGT 4600	300+/-50	346	200+/-20	Below	Below
KGT 4609	300+/-50	342	300+/-20	YES	Below
KGT 4639-C	500+/-50	506.5	440+/-20	YES	Below
KGT 4639-D	500+/-50	500	280+/-20	Below	Below
KGT-3841-3	500+/-50	518	480+/-20	YES	Below
KGT 3841-4	500+/-50	510	410+/-20	Below	Below

Melt wires of a known composition and melting temperature are another type of passive sensor discussed in this report. PIE is conducted on these wires to determine whether melting occurred, in turn indicating whether the corresponding melting temperature was reached (or exceeded). Selecting a suitable melt wire involves considering factors such as material composition, irradiation location, and compatibility with industry standards. Unfortunately, melt wires are limited in that they can only detect whether a single temperature has or has not been exceeded (i.e., whether the melt wire has melted or not). INL has been expanding the melt wire capabilities by investigating other methods of reading the melt wires during PIE and by implementing additive manufacturing techniques to miniaturize the packaging process.

The second objective of this report was to demonstrate proof of concept for the capacitance readout method of reading printed melt wires during PIE. Under the ASI program in FY-23, BSU proposed to perform that work; however, . In support of the BSU work, INL developed an AM ceramic package for encapsulating the new melt wires. Inks were synthesized at BSU that used new protocols rather than following previously established protocols implemented at INL, and testing at various temperatures was conducted at BSU to evaluate the melt behavior of the printed melt wires. The result was that the capacitance readout technique showed promise but also created more challenges than originally anticipated. For example, the tin synthesized at BSU showed unusual melting behaviors that did nothing to enhance the performance of the final printed melt wire prototype in terms of the capacitance readout method. To make the proof of concept work when applied to the printed melt wires, the ASI program would need to invest further resources and time. Consequently, the ASI program is not planning to continue this proof of concept work in FY-24, based on the progress and findings achieved in FY-23.

6. REFERENCES

[1] Pravdyuk, N. F., et al. “Investigation of Diamond and Silicon Carbide as Indicators of Irradiation Conditions.” *Proceedings of the International Conference Held at Berkeley Castle.* Vol. 46. 1961

[2] Snead, L. L., Williams, A. M., and Qualls, A. L. “Revisiting the use of SiC as a Post Irradiation Temperature Monitor.” *Effects of Radiation on Materials (2003).*

[3] Wilding, M. 2021. “Status of the Optical Dilatometer Method of Evaluating the Peak Irradiation Temperatures of SiC Passive Monitors.” Idaho National Laboratory. INL/EXT-21-65123. https://doi.org/10.2172/1894499.

[4] Rempe, J. L., et al. 2010. “Silicon Carbide Temperature Monitor Measurements at the High Temperature Test Laboratory.” Idaho National Laboratory, INL/EXT-10-17608. https://inldigitallibrary.inl.gov/sites/sti/sti/4460750.pdf.
[5] Campbell, A. A., Porter, W. D., Katoh, Y., & Snead, L. L. (2016). “Method for analyzing passive silicon carbide thermometry with a continuous dilatometer to determine irradiation temperature.” *Nuclear Instruments and Methods in Physics Research Section B: Beam Interactions with Materials and Atoms, 370,* 49-58.
[6] ASTM. 2018. “Standard Test Method for Melting And Crystallization Temperatures By Thermal Analysis.” American Standards for Measurement and Testing, ASTM E794-06. https://cdn.standards.iteh.ai/samples/100022/a0e1855ad61f4e6a9563a5e429e624ff/ASTM-E794-06-2018-.pdf.
[7] ASTM. 2023. “Standard Guide for Use of Melt Wire Temperature Monitors for Reactor Vessel Surveillance, E 706 (IIIE).” American Standards for Measurement and Testing, ASTM E 1214-11. https://www.astm.org/e1214-11.html.
[8] ASTM. 2018. “Standard Test Method for Temperature Calibration of Differential Scanning Calorimeters and Differential Thermal Analyzers.” American Standards for Measurement and Testing, ASTM E 967-18. https://www.astm.org/e0967-18.html.
[9] Pravdyuk, N. F., et al. 1962. “Diamond and Silicon Carbide as Indicators of Irradiation Conditions.” *D.J. Littler (Ed.),* International Conference on Properties of Reactor Materials and the Effects of Radiation Damage, Butterworths, Gloucestershire, England, 57–62.
[10] Bramman, J. I., Fraser, A. S., and W. H. 1971. “Temperature Monitors for Uninstrumented Irradiation Experiments.” *J. Nucl. Eng*. **25**, (6): 223–240.
[11] Suzuki, H., Iseki, T., and Ito, M. 1973. “Annealing Behavior of Neutron Irradiated b-SiC.” *J. Nucl. Mater*. **48**, (3): 247–252. https://doi.org/10.1016/0022-3115(73)90020-2.
[12] Palentine, J. E. 1976. “The Development of Silicon Carbide as a Routine Irradiation Temperature Monitor, and Its Calibration in a Thermal Reactor.” *J. Nucl. Mater.* **61**, (3): 243–253. https://doi.org/10.1016/0022-3115(76)90263-4.
[13] Rempe, J. L., et al. 2010. “Comparison Measurements of Silicon Carbide Temperature Monitors.” *IEEE Transactions On Nuclear Science*, **57**, (3). https://doi.org/10.1109/TNS.2010.2046333.
[14] Davis, K. L., et al. 2012. “Use Of Silicon Carbide Monitors In Atr Irradiation Testing.” Idaho National Laboratory, INL/CON-11-23899. https://www.osti.gov/servlets/purl/1055955.
[15] Davis, K. L., et al. 2012. “Melt Wire Sensors Available to Determine Peak Temperatures in ATR Irradiation Testing.” Eighth American Nuclear Society International Topical Meeting on Nuclear Plant Instrumentation, Control and Human-Machine Interface Technologies. Enabling the Future of Nuclear Energy. INL/CON-11-23913, Idaho National Laboratory. https://www.osti.gov/biblio/1054299.
[16] Mondal, K., Fujimoto, K., and McMurtrey, M. D. 2020. “Advanced Manufacturing of Printed Melt Wire Chips for Cheap, Compact Passive In-Pile Temperature Sensors,” *JOM*, **72**, (12): 4196–4201. https://doi.org/10.1007/s11837-020-04426-8.
[17] Mondal, K., Fujimoto, K., and McMurtrey, M. D. 2020. “Non-visual Analysis of Miniaturized Melt Wire Arrays for In-pile Measurement of Peak Irradiation Temperature.” Idaho National Laboratory, INL/EXT-20-57468. https://doi.org/10.2172/1668675.
[18] Hone, L., et al. 2021. “Design Optimization for Printed Melt Wire Arrays Encapsulation.” Idaho National Laboratory, INL/EXT-21-63886. https://doi.org/10.2172/1826589.
[19] Jewell, J. K., et al. 2017. “N-SERT (ISU-10537) Functional and Operational Requirements.” Idaho National Laboratory, FOR-301, Rev. 3.
[20] Jewell, J. K., et al. 2017. “Programmatic Thermal Analysis for the ISU-10537 Experiment.” Idaho National Laboratory, TEM-10200-1, Rev. 6.

Page left intentionally blank

Appendix A
PRINTED SENSOR TECHNOLOGY FOR HARSH ENVIRONMENTS

Page intentionally left blank

Appendix A
PRINTED SENSOR TECHNOLOGY FOR HARSH ENVIRONMENTS

Covering Period: April 2023 - December 2023

Date of Report: January 15th, 2024

POC(s): Dave Estrada (BSU), Mike McMurtrey (INL)

Work Package Team: Josh Eixenberger, Brian Jaques

Executive Summary and Highlights

SOW and Overview:

SOW: A limiting factor in current passive peak temperature monitoring melt wires is the readout technology. While much progress has been made to package and miniaturize melt-wire technology through additive manufacturing techniques, current e-beam welded stainless steel packaging limits RF readout of melt wire chips. Visual inspection is also not an option, while micro-CT for post irradiation examination remains inaccessible and cost prohibitive. In this task we will work with INL to develop an additive manufactured ceramic package for passive peak temperature sensors. Inks will be synthesized following previously established protocols, and the high temperature testing will be conducted to evaluate the melt behavior of the passive sensors. An electrical readout scheme will be developed to either (a) read the sensors from within the package, or (b) recover the sensor chips and read them out of the package. In addition, preliminary investigations into melt capacitors will be conducted. A stack of melt discs that constitute parallel plates of capacitors will be printed from the afore mentioned inks. By stacking the disks inside the package, we will create a series connected capacitor that can be electronically connected to an LCR meter to read the final capacitance of the stack. Careful design of the melt discs will enable us to use a simple series capacitance model to determine which capacitors have failed and which discs remain intact. ***Success criteria*** are (1) Deliver a prototype melt capacitor device with ceramic packaging (2) deliver a simple model validated against initial thermally cycled devices. ***Risk mitigation***. We will compare electrical data to more complex micro-CT imaging and COMSOL models to help validate the technique as needed.
Overview: For this project, three materials were selected for ink formulation, printing, and device testing to demonstrate proof of concept: Indium (melting point- 156.6° C), Tin (melting point- 231.9° C), and Zinc (melting point- 419.5° C). The ceramic packaging was designed, and 3D printed by INL with a lid that has two feedthroughs for electrical contact. The target substrates chosen were silicon dioxide, sapphire, and the 3D printed ceramic packaging as the printing and melting behavior may differ due to substrate interactions and differences in surface roughness.

Results:

Nanoparticle Ink formulation: An indium nanoparticle ink was purchased from ANI. To formulate tin and zinc nanoparticle inks, nanoparticles were purchased from US nanomaterials, with a size range of ~60 nm and are capped with PVP. To evaluate melting characteristic and determine the PVP content of the as-received nanoparticles, the tin nanoparticles were evaluated with TGA in N_2 atmosphere. As seen in Figure A-1, the DSC peak shows a sharp peak near 240° C as expected for the melting point of tin. PVP is expected to undergo a thermal decomposition at ~250-450° C depending on environmental conditions.

However, there was a slight mass gain above the melting point of tin, indicating a possible small leak in the gas supply line inducing oxidation of tin or a possible nitrate formation.

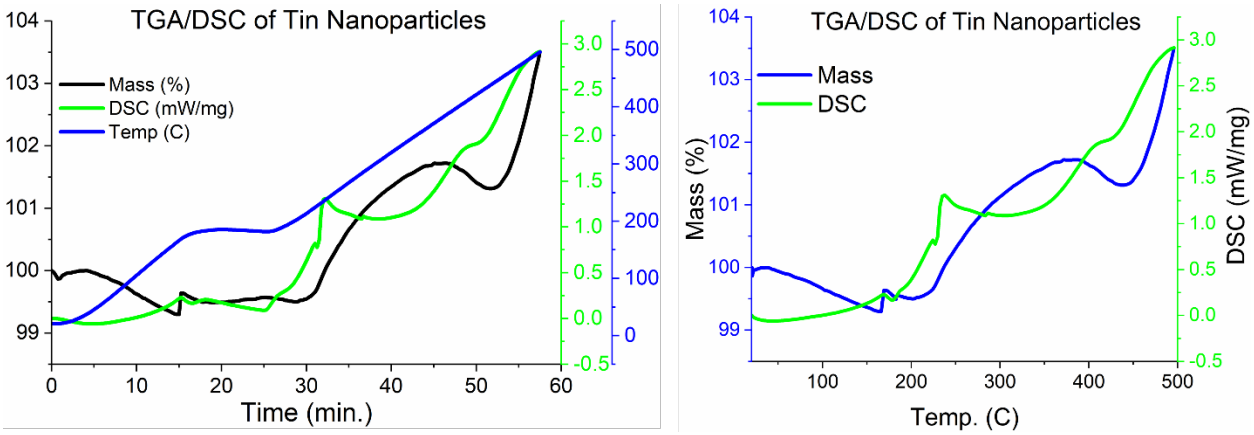

Figure A-1. TGA/DSC of Tin nanoparticles (melting point 232 °C) in N_2 atmosphere. (Left) TGA/DSC data with time as the x-axis. Measurement conducted with an isotherm at 175 °C for 10 minutes. Chose isotherm at 175 °C as target sintering temperature due to PVP melting point at ~150 °C. (Right) Same data without the isotherm and temperature as the x-axis to estimate PVP content from decomposition. The DSC shows a peak at ~232 °C indicative of Tin's melting point. Unexpectedly, the sample gained mass as the sample was heated to 500 °C. Possible nitridation from N_2 atmosphere (unlikely- Tin Nitride unstable) or oxidation due to leak in gas line or from decomposition of PVP possibly forming tin nitrate.

For nanoparticle inks to be printable with the aerosol jet printer, the nanoparticle size needs to be below 100 nm and the rheological requirements of the printer need to be met. Through our previous studies on various co-solvent systems, we have determined a combination of water, ethanol (10-20%), and ethylene glycol (up to 30%) as a suitable system to match the rheological requirements of the printer. To verify the size range of the purchased nanoparticles, SEM was performed. As seen in Figure A-2. , while a good majority of the nanoparticles have diameter of less than 100 nm, some larger (> 2 µm) particles are present that may clog the nozzle of the printer. To ensure a printable ink, the nanoparticles were suspended in ethylene glycol, centrifuged at 6,000 RPM for 5 minutes, and the supernatant was collected. The supernatant was then centrifuged at 21,000 rpm for 10 minutes to pellet the smaller particles and resuspended in the ink's co-solvents to generate a printable ink.

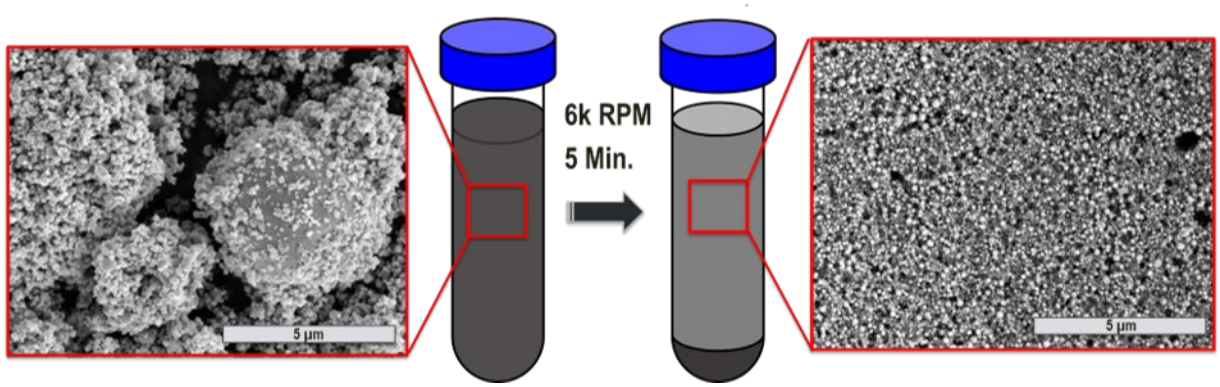

Figure A-2. As-received Sn nanoparticles had a large size distribution with many particles > 1 µm. To formulate a printable ink, the larger particles were separated via centrifugation and resuspended into final ink formulation. SEM images were collected before and after size separation to confirm removal of large particles.

Once the inks were formulated, the nanoparticles inks were printed with an Optomec aerosol jet printer. The IDEs (Figure 3) were printed with large contact pads to ensure good contact with the electrical feedthroughs and were printed with ~100 µm wide fingers. Both the tin and the zinc nanoparticle inks were printed in silicon dioxide and directly printed on the ceramic packaging base. Printing on the silicon dioxide yielded high quality prints near the target size range with minimal overspray. The prints on the ceramic packaging were still successful but the line quality was impacted, with more overspray and a less consistent deposition of the material in the lines. This is most likely due to the higher surface roughness of the 3D printed ceramic. However, printing on coupons, such as SiO_2 or sapphire is still a viable route as the coupons can be placed in the ceramic capsule if the electrical feedthroughs on the lid are aligned with the contact pads of the printed IDE. After printing of the devices, the tin IDEs were sintered at 200° C for 30 minutes in an argon atmosphere. Similarly, the zinc IDEs were sintered for 30 minutes in an argon atmosphere but were sintered at 400°C.

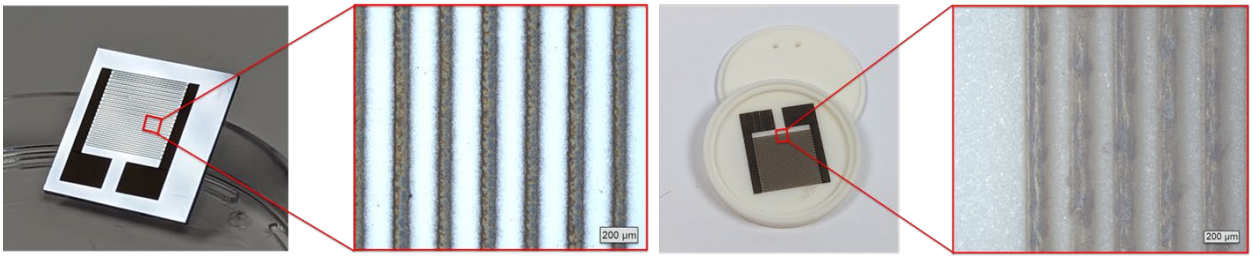

Figure A-3. Sn inks were printed on SiO_2 (left) and the additively manufactured ceramic package (right) to understand device performance on different substrates and within the ceramic package. Prints on the SiO_2 yielded devices with more consistently deposited nanoparticles with minimum overspray when compared with the prints on the ceramic capsule.

Capacitance measurements of IDEs: To validate melting behavior, continuously monitor the capacitance, and make visible observations of the printed IDE structures, an electrical feedthrough for a tube furnace was fabricated. To make an electrical feed through, a ¼" alumina bore tube was used. Steel wiring was fed through the bore holes and alligator clips with a flat clip were utilized to connect the steel wiring to the contact pads of the printed IDEs.

A viton o-ring was placed on the alumina tube, the exposed end sealed with high temperature silicone, and then was then fed through the thermocouple access port. Initial capacitance of the tin IDE was ~28.0 pF. To test the performance in the tube furnace, the tube was first brought under vacuum and then a continuous flow of argon (250 sccm) was introduced to ensure an inert atmosphere, preventing oxidation of the metals at elevated temperatures. The furnace was programed to ramp at 10°C per minute and dwelling for 5 minutes every 25 C to take capacitance measurements. During the experiment, the capacitance of the IDEs increased to XX pF. However, even at 25 C above the melting point of tin, the fingers didn't melt into each other, shorting the capacitor as expected. The experiment was duplicated but ramped up to 375 C, nearly 150 C above the melting point of tin to ensure melting of the tin metal and for follow up visual evaluations of the printed IDEs.

Status: Ongoing. Due to the lack of the tin's IDE fingers melting into each other and causing a short of the device, the zinc IDEs are currently being tested. Upon validation of the results, alternative geometries and/or melting devices schemes will be investigated.

Changes/Problems:

The indium ink purchased from ANI inc. agglomerated during storage (~1-2 months) inside of the glovebox, making it unprintable with the jetting printers.

Tin and zinc nanoparticle ink formulation was successfully completed and validated though printing of interdigitated electrodes (IDE) structures. These devices were successfully printed on silicon dioxide

and the 3D printed ceramic substrates fabricated at INL for packaging of the sensors. However, the melt characteristics of the printed tin structures didn't behave as anticipated. Capacitive measurements were conducted on the tin (melting point- 231.9 C) IDE up to 375 C and the fingers of the IDEs didn't spread upon melting, inducing the expected shorting of the device. This is likely due to the thin film produced via printing with the aerosol jet printer and the surface tension of the melted tin. This may be overcome by printing thicker fingers, providing enough material to allow enough spread from the fingers to short the IDE. These results are being validated with the zinc prints to determine if the same results are achieved or if this is an artifact of this device design and/or material. Work is continuing to demonstrate proof of concept of this strategy but alternative concepts for real-time monitoring of target temperatures are being considered.